Quantifying canopy fractional cover and change in Fanjingshan National Nature Reserve, China using multi-temporal Landsat imagery

Yu Hsin Tsai, Douglas Stow, Lei Shi, Rebecca Lewison & Li An

Published online: 27 Apr 2016.

Submit your article to this journal ↗

View related articles ↗

View Crossmark data ↗

Taylor & Francis
Taylor & Francis Group

Quantifying canopy fractional cover and change in Fanjingshan National Nature Reserve, China using multi-temporal Landsat imagery

Yu Hsin Tsai[a], Douglas Stow[a], Lei Shi[b], Rebecca Lewison[c] and Li An[a]

[a]Department of Geography, San Diego State University, San Diego, CA, USA; [b]Fanjingshan National Nature Reserve Administration, Guizhou, China; [c]Department of Biology, San Diego State University, San Diego, CA, USA

ABSTRACT

This letter explores factors affecting the quantification and mapping of forest canopy fractional cover (CFC), and explores causes of CFC change. CFC was quantified using a simple linear mixture model based on the modified soil-adjusted vegetation index (MSAVI) derived from Landsat TM surface reflectance data of Fanjingshan National Nature Reserve (FNNR) in China. Different soil and vegetation endmembers were tested to analyse the sensitivity of the mixture model. Illumination effects due to topographical variability are found to influence MSAVI and therefore CFC estimates. Implementing an illumination stratification that selects different closed canopy endmembers for different topographic-related illumination strata generally minimizes these effects. The spatial distribution and possible causes of CFC change were examined. Most changes in CFC over the 15-year study period appear to have resulted from anthropogenic activities, at least based on the precision constraints of Landsat-derived CFC change estimates and limited high spatial resolution imagery used in a mostly visual verification of patches with low CFC and reduction in CFC between image dates.

1. Introduction

Fanjingshan National Nature Reserve (FNNR) in Guizhou province, China was established in 1978 and was recognized as a UNESCO Biosphere Reserve in 1986 (Wu et al. 2004). FNNR serves as a critical conservation area and the only habitat for an endemic species of the Guizhou snub-nosed monkey (*Rhinopithecus brelichi*) (Wu et al. 2004). Throughout China and in lands immediately adjacent to the FNNR, citizens have planted trees in sloped lands that were formally farmed as part of the Grain to Green Programme (GTGP), which was implemented at FNNR around 2001–2002 (Feng et al. 2005). This type of payment for ecosystem services (PES) policy is intended to encourage tree planting in sloped land as a means to reduce soil erosion and stream flooding (Feng et al. 2005). The impacts of human activities (e.g., tourism and agriculture) and natural disturbances (e.g.,

landslides) on the forest vegetation that is primary habitat for *R. brelichi* have not been well documented in this area; neither has the expansion of reforested lands associated with PES policy and subsequent logging of trees in afforested zones.

Satellite remote sensing provides a means for retrospective analyses of changes in forest cover at FNNR (as elsewhere worldwide), as well as for monitoring future changes in response to government policies, management practices and human activities. Airborne imaging missions have not occurred in the past and are prohibitively expensive and may not be permitted by governmental agencies. Factors such as persistent cloud cover, monsoonal climate, steep terrain, and varying forest community composition make satellite remote sensing at FNNR challenging. Synthetic aperture radar (SAR) imagery can 'see through' cloud cover and most precipitation, but the steep terrain of FNNR and side-looking illumination geometry make forest cover sensing with satellite SAR data intractable (Kellndorfer et al. 2014). Factoring in duration of image archive, sufficient spatial resolution for resolving forest cover on relative small slope facets, high spectral-radiometric fidelity, and free access to geometrically and radiometrically processed image products, the satellite optical imaging system of greatest promise is Landsat.

A number of modelling approaches to estimating the fraction of forest cover based on Landsat multispectral imagery have been tested and implemented (e.g., Asner et al. 2005; Rogan et al. 2008; Hansen et al. 2013). These approaches primarily fall within the categories of image classification (cover interval classes), spectral mixture analysis, and continuous value machine learning routines. A parsimonious modelling approach to estimating forest fractional cover is a simple, two-component (forest and bare ground) linear mixture model based on spectral vegetation index input. Wang, Qi, and Cochrane (2005) tested such a model with Landsat Enhanced Thematic Mapper Plus (ETM+) data for Brazilian Amazon rainforest and achieved a high degree of success in mapping canopy fractional cover (CFC). They found that unmixing pixels using the modified soil adjusted vegetation index (MSAVI) (Qi et al. 1994) as input achieved the most accurate results and that MSAVI was mostly linearly related to CFC variation. Sader et al. (1989) and Jiang, Wang, and Wang (2010) determined that the accuracy of vegetation monitoring in areas of rugged terrain can be influenced by topographic illumination effects, even when based on time series of spectral vegetation indices.

The objectives of this letter are to explore the utility and sensitivity of a relatively simple pixel unmixing approach developed by Wang, Qi, and Cochrane (2005) and to map and qualitatively analyse CFC changes within the FNNR and its environs accordingly. The steep terrain and varying vegetation cover in FNNR pose challenges to mapping forest cover compared to the Amazonian rainforest in the previous study (Wang, Qi, and Cochrane 2005). In order to develop a relatively simple approach to monitoring forest cover, the sensitivity of CFC estimates to the selection of maximum canopy and bare ground end-members, and stratification of terrain-related illumination zones is explored. Furthermore, Landsat-derived CFC maps are compared to a vegetation community type GIS layer and a Pleiades image in Google Earth to identify possible causes of CFC change.

2. Data and methods

Relatively cloud-free Landsat 5 Thematic Mapper (TM) and Landsat 7 ETM+ data from the Landsat Ecosystem Disturbance Adaptive Processing System (LEDAPS) surface

reflectance product for Path 126, Row 41 of the Worldwide Reference Systems were downloaded from the U.S. Geological Survey Earth Explorer website (http://earthex plorer.usgs.gov/). Images with less than 5% cloud cover were identified from all available summer (June–September) acquisitions from 1990 forward, and two Landsat 5 TM images, out of the 10 images that met the cloud cover criterion, were selected for analysis for mid-1990 and early 2010 periods. This time span allows us to examine canopy forest cover prior to and after the implementation of GTGP. The first image was captured on 22 August 1996 and the second date was on 16 August 2011, with 0.1 and 4% cloud cover, respectively. Summer (August) dates were selected to ensure maximum leaf development within deciduous and mixed deciduous-evergreen forest types and to minimize terrain shadows in the mountainous study area. Subset images 27 km (E–W) by 28 km (N–S) containing FNNR and its surrounding area for each date were extracted. Figure 1 shows the image subset extent of the FNNR study area with Landsat LEDAPS surface reflectance image from 2011.

A vegetation community type GIS layer and a high spatial resolution satellite image in Google Earth were used for comparison of forest cover to canopy cover estimation. The unpublished vegetation map, created through a Global Environmental Facility (GEF) and FNNR administrative collaborative project from 2007 to 2012, contains nine general community types, which were aggregated into five functional type categories: deciduous, evergreen, mixed deciduous-evergreen, afforested bamboo and afforested conifer. The Google Earth image was captured by the Pleiades satellite on 26 October 2013 and
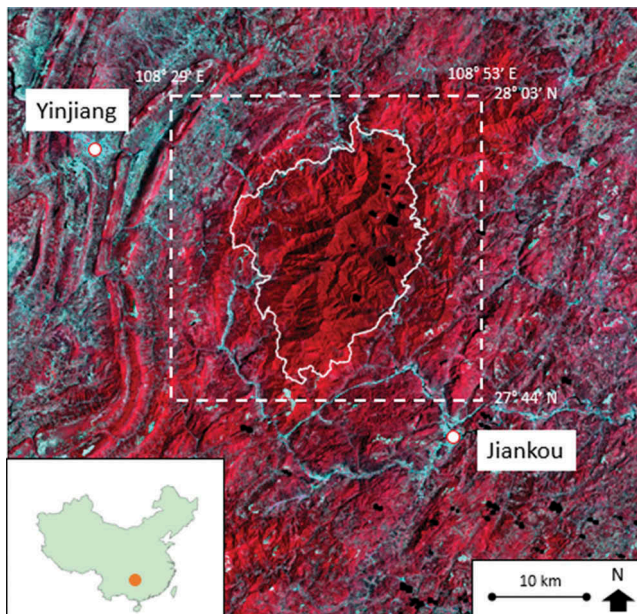
Figure 1. Study area of Fanjingshan National Nature Reserve (FNNR) and its surrounding area. The false colour infrared image is derived from the Landsat LEDAPS surface reflectance image product of 2011 from Landsat 5. The study area is delineated by a white dotted line with the reserve boundary as a white solid line. The general location of FNNR on the map of China is symbolized by an orange circle.

has 0.5 m spatial resolution. The image extent covers the FNNR and its environs and is one of the few high spatial resolution satellite images available for this rural, cloud prone area. Note that the Pleiades image was collected in 2013, more than 2 years after the second (time = 2) Landsat image date, and could indicate different CFC in some areas relative to 2011 conditions. The extremely dense tree cover (i.e., predominantly high CFC) in FNNR makes it challenging to use the single-date Pleiades image as a reference source for quantifying canopy cover (Carreiras, Pereira, and Pereira 2006), but it was useful for visually identifying areas of low CFC.

CFC was calculated and mapped using the two Landsat images and the following equation:

$$CFC = \frac{V_{pixel} - V_{open}}{V_{canopy} - V_{open}} \tag{1}$$

where V is a spectral vegetation index value for a given pixel and *open* and *canopy* represent pure bare soil and densest forest endmembers, respectively (Wang, Qi, and Cochrane 2005). After testing multiple spectral vegetation indices and surface reflectance bands, MSAVI derived by LEDAPS was utilized as the vegetation index for CFC modelling, as it was found to be most sensitive to and vary linearly with CFC (as was the case for Wang, Qi, and Cochrane 2005). The particular formulation of MSAVI is based on Qi et al. (1994) and is calculated with the red and NIR surface reflectance bands (i.e., ρ_{NIR} and ρ_{red}) using the following Equation (2):

$$MSAVI = \frac{2\rho_{NIR} + 1 - \sqrt{(2\rho_{NIR} + 1)^2 - 8(\rho_{NIR} - \rho_{red})}}{2} \tag{2}$$

Image endmembers were selected using feature space plots between red and NIR bands, along with corresponding MSAVI values. The densest vegetation pixels were selected from near the tasseled part of the red-NIR scatterplot and having the top 99% MSAVI values to represent *canopy* endmembers. Three different bare soil endmembers of varying soil brightness were selected based on low, medium, and high positions along the soil line of the red-NIR scatterplot, and the bottom 1% MSAVI values were utilized to represent the *open* endmembers. Endmember pixels were reviewed on Landsat and Pleiades imagery to ensure the selection only included true forest and bare soil features. The *canopy* endmember selected from the entire study area combined with the darkest, brightest, and mid-range soil endmembers were utilized to derive CFC maps. The sensitivity of CFC estimates to different endmembers was reviewed by comparing their quantitative ranges.

A DEM that has 30 m spatial resolution and 20 m vertical accuracy generated from stereo image data of NASA Terra ASTER satellite system was utilized to generate synthetic illumination and annual irradiance rasters, to examine the relationships between solar irradiance at time of imaging and total annual solar irradiance with MSAVI and CFC distributions. For these purposes and given the scale of analysis, the ASTER DEM has sufficient resolution and accuracy. The synthetic illumination image was created based on the time and sun angle when the Landsat TM image data were captured. The annual radiance image was created for an entire annual cycle.

A standard and a stratified approach for endmember selection and mixture modelling were tested to estimate canopy cover. The standard approach utilized one *canopy* and one *open* image endmember for each date. For the stratified approach, three image strata were generated for each date based on three terrain-influenced illumination strata: (1) shaded pixels (mostly northwest-facing slopes), (2) directly illuminated pixels (mostly southeast-facing slopes), and (3) other (mostly flat, northeast- and southwest-facing slopes). Shaded pixels were determined through an unsupervised *k*-means clustering and classification routine using all spectral bands. Ten classes were generated and the three classes with the lowest spectral signature were treated as the shaded stratum. Sunny pixels were captured based on the synthetic illumination image and the pixels within 45° of direct sunlight on either direction. Pixels that were not classified as shaded or sunny were treated as the third ('other') stratum. Canopy cover was estimated for each stratum, then merged to form a single CFC map.

CFC values were calculated for different dates of Landsat images separately. A *CFC* change (Δ*CFC*) map was created by temporal differencing *CFC* values between two dates (i.e., t_1 and t_2) as follows:

$$\Delta\text{CFC} = \text{CFC}_{t_2} - \text{CFC}_{t_1} = \left(\frac{V_{\text{pixel}t_2} - V_{\text{open}t_2}}{V_{\text{canopy}t_2} - V_{\text{open}t_2}}\right) - \left(\frac{V_{\text{pixel}t_1} - V_{\text{open}t_1}}{V_{\text{canopy}t_1} - V_{\text{open}t_1}}\right) \quad (3)$$

3. Results

A parsimonious linear mixture modelling approach to estimating CFC and monitoring change in CFC was tested, based on MSAVI images as input to the mixture model represented by Equation (3). Table 1 shows the image endmembers and quantitative ranges of CFC maps derived from the standard and terrain-stratified approaches. Maps generated using bright soil endmembers have lower minimum CFC values and quantify more realistic cover percentages for bare ground/open canopy. Figure 2(a) shows the CFC map generated with the 1996 Landsat 5 image using bright soil as an *open* endmember; Figure 2(b) shows the CFC map generated with the same image using the terrain-stratified approach. Note that non-forested pixels such as urban area and farmland are excluded from CFC estimation by applying a binary forest/non-forest mask. The binary mask was generated based on the 1996 Landsat image with an unsupervised image classification routine and a 3 × 3 majority filter applied to reduce fine-scale classification noise.

Table 1. Image endmember (EM) values of MSAVI and quantitative range of canopy fractional cover (CFC) maps. Standard (non-stratified) approach utilizes single canopy endmember and dark/medium/bright soil endmembers (order as appears). Stratified approach utilizes multiple canopy endmembers (values shown as shaded/other/directed illuminated) and their associated bright soil endmember. MSAVI values of canopy and open endmembers are scaled by 10,000. CFC values represent the percentage of canopy cover for a given pixel. Minimum and maximum values that are < 0 and > 100% stem from the unconstrained mixing model.

	Model type	Canopy EM	Open EM	Mean (%)	Median (%)	Minimum (%)	Maximum (%)
1996	Standard	7873	292/469/693	57/56/54	58/57/55	−3/−6/−9	100/100/100
	Stratified	5318/7865/8100	367/667/860	68	67	−2	103
2011	Standard	7529	410/536/720	60/59/58	61/61/60	−5/−7/−10	100/100/100
	Stratified	4880/7458/7530	383/718/854	69	69	−5	101
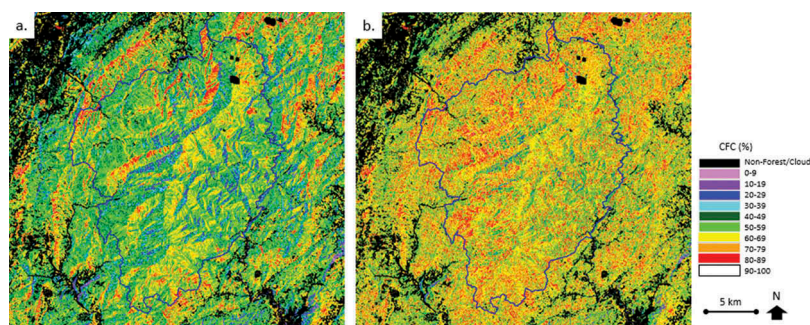
Figure 2. Canopy fractional cover maps derived from 1996 Landsat 5 surface reflectance image. a. Standard approach using deciduous image endmember as canopy and bright soil endmember as open and b. terrain-stratified approach.

Quantitative ranges of CFC maps generated using multiple canopy endmembers for the three strata are also shown in Table 1. The stratified CFC maps were generated based on three illumination strata and their associated canopy endmembers, together with the open endmember of bright soil. The 2011 CFC map shows a slight (1%) CFC increase compared to the 1996 CFC map; it also has a wider range (1% more) of CFC values.

CFC maps derived from the standard and stratified approaches for the same Landsat image were compared with image differencing. Figure 3(a,b) shows the CFC difference map derived from the standard and terrain-stratified products for 1996 and 2011, respectively. Image mean and median values for the stratified maps are consistently higher than the standard maps as seen in Table 1, for both dates and all three soil endmembers. From the difference images, directly illuminated (southeast facing) slopes show almost identical CFC values between the standard and stratified approaches; shaded (west and north facing) slopes have up to 30% higher CFC values through the stratified approach compared to the standard approach for both dates as observed in Figure 3(a,b). The mean values of the two CFC difference maps are 13.57 and 12.94, respectively, also indicating the overall higher CFC values from the stratified approach.

CFC difference maps generated from 1996 and 2011 CFC maps derived using both standard and stratified approaches are shown in Figure 3(c,d). Almost half of the pixels (45%) exhibit minimal change with between 5% increase and 5% decrease in CFC. The mean values for the standard and stratified CFC difference maps are 4.36 and 2.32, respectively. The difference map from the stratified approach exhibits a greater range in CFC differences than the standard approach, particularly for areas in topographic shadows, as seen in Figure 3(d). In general, apparent CFC increases up to 20% on most of the shaded (west and north facing) slopes within the reserve, with southeast-facing slopes showing less of an apparent increase.

CFC change maps were compared to the generalized vegetation community map and found small CFC differences in all types of vegetation cover. Based on field observations in FNNR, evergreen vegetation in general grows slow and canopy density increases overtime; deciduous vegetation grows faster while canopy density is more constant. The patterns observed on CFC change maps match our team's field observations. Mixed deciduous-evergreen vegetation coincides with the minor CFC change. Areas of greater

CFC Change (%)
- --46
- -45--36
- -35--26
- -25--16
- -15--6
- -5 to 5
- 6-15
- 16-25
- 26-35
- 36-45
- 46+
- Non-Forest/Cloud

10 km   N
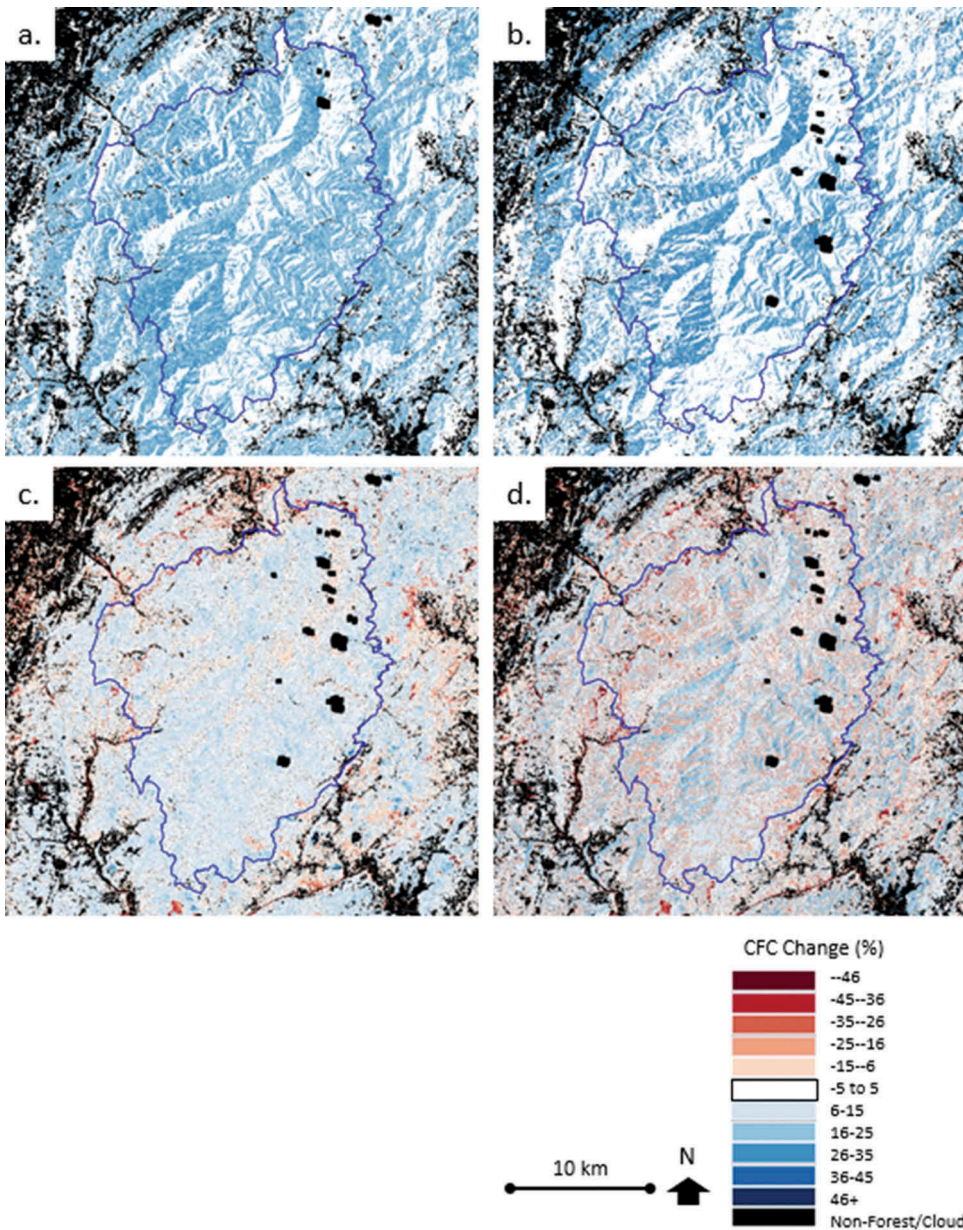
Figure 3. Canopy fractional cover difference maps. a. Terrain-stratified product minus standard product for 1996, b. terrain-stratified product minus standard product for 2011, c. standard approach 2011 minus 1996 and d. terrain-stratified approach 2011 minus 1996.

CFC increase coincide with evergreen types. Farmland and afforested-bamboo cover types are associated with CFC decrease.

Changes indicated on CFC change maps were compared to the October 2013 Pleiades image in Google Earth to identify possible causes of CFC increase and decrease. On the west and north side of the reserve, more dramatic CFC reduction is associated

with the highway development and agricultural activities near villages. The highway was constructed from 2007 to 2010, and cuts in and out of the reserve boundary into its buffer zone. Along the paved highway, associated landslide scars caused CFC to decrease by 50% as shown in Figure 3(c,d). This CFC decrease is more exaggerated through the stratified approach, which indicates up to 60% CFC reduction. Agriculture land parcels converted to conifer and tea trees through the PES programme mostly reflect moderate CFC increase of 20%, and up to 40% in some areas in the north. Patches of CFC decrease up to 20% coincide with terraces of non-PES agriculture activities, and man-made structures such as villages and temples, mostly at lower elevations in the reserve buffer area.

4. Discussion and conclusions

Key contributions of this letter are: (1) testing the Wang, Qi, and Cochrane (2005) mixture model for estimating CFC in a different study area and forest change context, (2) demonstrating that the illumination stratification approach effectively minimizes terrain shading effects on MSAVI and therefore CFC estimates, while avoiding potential artefacts associated with DEM-based terrain corrections, and (3) showing that anthropogenic activities are the primary causes of changes in CFC during the study period based on derived CFC change maps and limited high spatial resolution imagery. Though persistent cloud cover and steep terrain make satellite-based monitoring of CFC challenging in this study area, our results suggest that both natural and anthropogenic disturbance effects on the natural forest, and planting and harvesting of PES plots can be effectively tracked over time.

Our analyses revealed anthropogenic activities are apparent causes of CFC changes in FNNR during the study period. Road network development and agricultural activities were observed through CFC change maps. Results suggest that PES land experiences roughly 15% CFC increase, while regular agriculture activities mostly led to CFC reduction. CFC changes could also be contributed to climate and precipitation variations, tree mortality, etc. Precipitation data are not available at this time, and further fieldwork would be needed to verify the non-anthropogenic related causes.

In general, CFC values show a low sensitivity to different endmember values in terms of soil brightness. The three soil brightness endmembers that were tested during the standard approach resulted in 5–6% difference in CFC minimum values, as seen in Table 1. Different soil endmembers resulted in a 3% difference in CFC mean values, indicating minor sensitivity to *open* endmember values. CFC values show greater variation to different *canopy* endmembers that were tested between the standard and stratified approaches. The mean values of CFC maps are up to 14% higher with the use of illumination strata compared to the standard approach. This is mainly due to higher and more realistic CFC estimates in the shaded regions that exhibit lower MSAVI values (i.e., not completely normalized) from the lack of direct solar illumination. Without stratification by illumination zones, CFC values are generally 30–40% lower on shaded slopes, even though CFC visually appears to be as high or higher on the Pleiades image in Google Earth. The illumination stratification approach considers high and low illuminated slopes separately and thus increases CFC values in the shaded regions to minimize these topographic effects.

Another stratification scheme based on vegetation community type was tested in addition to the illumination stratification approach. Using vegetation community types to generate various image endmembers yielded almost identical CFC maps to those from the standard approach, as closed-canopy endmembers were similar between vegetation types. The above inferences together lead to a conclusion that the illumination stratification approach worked well for quantifying CFC in FNNR.

This Letter demonstrates that Landsat TM imagery and a simple CFC mixture model enable quantification of forest canopy cover and have the potential to be used to map and monitor landslides, logging, growth of PES vegetation plots, and regrowth of native forests. Some of the challenges in utilizing Landsat imagery for estimating CFC and monitoring CFC changes are the high frequency of cloud cover in the region, topography and illumination, snow, field hazards that limit field validation during the summer (full leaf-on season), and vegetation phenology. These characteristics of the FNNR region are different from the Brazilian Amazonian rain forests where Wang, Qi, and Cochrane (2005) developed the simple pixel unmixing model. Very few, mostly cloud-free Landsat images are available for FNNR, particularly during the summer monsoonal rain season. It is even more challenging to find cloud-free imagery that was captured on near-anniversary dates. A three-date, 18-band Landsat image composite was utilized to map forest variables (Franco-Lopez, Ek, and Bauer 2001) in order to overcome cloud cover issues and capture all phenological variability; this type of multi-date mapping approach could be helpful in regions such as FNNR. High spatial resolution satellite imagery is also very limited. The mountainous terrain influences extensive zones of shadow and can influence the accuracy on CFC estimation.

Note that for relatively stable satellite image time series such as terrain-corrected surface reflectance products, endmember values can be considered stable for bi-temporal image pairs (i.e., $V_{\text{canopy } t1} = V_{\text{canopy } t2}$ and $V_{\text{open } t1} = V_{\text{open } t2}$) and Equation (3) simplifies to:

$$\Delta\text{CFC} = \frac{V_{\text{pixel } t_2} - V_{\text{pixel } t_1}}{V_{\text{canopy}} - V_{\text{open}}} \tag{4}$$

Future research will need to focus on comparing CFC estimates to ground-based digital hemispherical photography (DHP) to better characterize their accuracy and reliability. DHP is a widely used optical measurement to derive ground-based estimation of forest structural attributes (Pueschel, Buddenbaum, and Hill 2012). Furthermore, the utility of simplified derivation of CFC change (i.e., Equation (4)) will be tested. Additional efforts are also needed to develop and test time series image composite approaches that utilize all available imagery and minimize issues such as cloud cover and exploit vegetation phenology associated with forest composition differences.

Acknowledgements

Disclosure statement

No potential conflict of interest was reported by the authors.

Funding

References

Asner, G. P., D. E. Knapp, A. N. Cooper, M. M. Bustamante, and L. P. Olander. 2005. "Ecosystem Structure Throughout the Brazilian Amazon from Landsat Observations and Automated Spectral Unmixing." *Earth Interactions* 9 (7): 1–31. doi:10.1175/EI134.1.

Carreiras, J. M., J. M. Pereira, and J. S. Pereira. 2006. "Estimation of Tree Canopy Cover in Evergreen Oak Woodlands Using Remote Sensing." *Forest Ecology and Management* 223 (1–3): 45–53. doi:10.1016/j.foreco.2005.10.056.

Feng, Z., Y. Yang, Y. Zhang, P. Zhang, and Y. Li. 2005. "Grain-For-Green Policy and Its Impacts on Grain Supply in West China." *Land Use Policy* 22: 301–312. doi:10.1016/j.landusepol.2004.05.004.

Franco-Lopez, H., A. R. Ek, and M. E. Bauer. 2001. "Estimation and Mapping of Forest Stand Density, Volume, and Cover Type Using the K-Nearest Neighbors Method." *Remote Sensing of Environment* 77 (3): 251–274. doi:10.1016/S0034-4257(01)00209-7.

Hansen, M. C., P. V. Potapov, R. Moore, M. Hancher, S. A. Turubanova, A. Tyukavina, D. Thau, et al. 2013. "High-Resolution Global Maps of 21st-Century Forest Cover Change." *Science* 342: 850–853. doi:10.1126/science.1244693.

Jiang, H., X. Wang, and Q. Wang. 2010. "Vegetation Monitoring in Rugged Terrain with One Novel Topography-Adjusted Vegetation Index (TAVI)." *IEEE Image and Signal Processing* 5: 2294–2297.

Kellndorfer, J., O. Cartus, J. Bishop, W. Walker, and F. Holecz. 2014. "Large Scale Mapping of Forests and Land Cover with Synthetic Aperture Radar." In *Land Applications of Radar Remote Sensing*, edited by F. Holecz, P. Pasquali, N. Milisavljevic, and D. Closson, 59–94. Rijeka: InTech.

Pueschel, P., H. Buddenbaum, and J. Hill. 2012. "An Efficient Approach to Standardizing the Processing of Hemispherical Images for the Estimation of Forest Structural Attributes." *Agricultural and Forest Meteorology* 160: 1–13. doi:10.1016/j.agrformet.2012.02.007.

Qi, J., A. Chehbouni, A. R. Huete, Y. H. Kerr, and S. Sorooshian. 1994. "A Modified Soil Adjusted Vegetation Index." *Remote Sensing of Environment* 48: 119–126. doi:10.1016/0034-4257(94)90134-1.

Rogan, J., J. Franklin, D. Stow, J. Miller, C. Woodcock, and D. Roberts. 2008. "Mapping Land-Cover Modifications over Large Areas: A Comparison of Machine Learning Algorithms." *Remote Sensing of Environment* 112 (5): 2272–2283. doi:10.1016/j.rse.2007.10.004.

Sader, S., R. B. Waide, W. T. Lawrence, and A. T. Joyce. 1989. "Tropical Forest Biomass and Successional Age Class Relationships to a Vegetation Index Derived from Landsat TM Data." *Remote Sensing of Environment* 28: 143–198. doi:10.1016/0034-4257(89)90112-0.

Wang, C., J. Qi, and M. Cochrane. 2005. "Assessment of Tropical Forest Degradation with Canopy Fractional Cover from Landsat ETM+ and IKONOS Imagery." *Earth Interactions* 9 (22): 1–18. doi:10.1175/EI133.1.

Wu, G., H. Wang, H. Fu, J. Zhao, and Y. Yang. 2004. "Habitat Selection of Guizhou Golden Monkey (Phinopithecus Roxellanae Brelichi) in Fanjing Mountain Biosphere Reserve, China." *Journal of Forestry Research* 15 (3): 197–202. doi:10.1007/BF02911024.